Computers and Geotechnics 130 (2021) 103924

Contents lists available at ScienceDirect

Computers and Geotechnics

journal homepage: www.elsevier.com/locate/compgeo

Research Paper

Performance-based analysis of cantilever retaining walls subjected to near-fault ground shakings

Milad Aghamolaei, Alireza Saeedi Azizkandi *, Mohammad Hassan Baziar, Sadegh Ghavami

School of Civil Engineering, Iran University of Science and Technology, Tehran, Iran

ARTICLE INFO

Keywords:
Near-fault
Performance-based analysis
Wavelet approach
Frequency content

ABSTRACT

Considering the devastating damages of 'forward-directivity' on structures, a series of finite element models were conducted to evaluate the seismic performance of cantilever retaining walls under near-fault excitations. The wavelet approach was used to extract the velocity pulse of near-source motions, and a semi-artificial records reagent far-field earthquake was produced. Both were then imposed on the model, separately. The results indicated a vivid difference in lateral displacement, in which some cases up to differences of experienced 85% and forces along the walls were approximately equal. In view of this finding, a wide range of PGAs was applied to the near-fault scenarios of the models. The captured movements were compared with the recommended criteria for performance-based aseismic design of retaining structures. According to the numerical analysis, in most earthquakes, for accelerations exceeding 0.4 g, lateral displacement of the wall had a higher value than the permissible proposed limits. Also, accelerations exceeding 0.6 g for both near and far-field records resulted in wall failure (>5% H). The final section of this research presents a comprehensive parametric study on the effects of ground motion characteristics and soil mechanical properties on system performance.

1. Introduction

Earthquake ground motions recorded close to a fault plane recognized as near-fault ground motions can be extremely different from motions captured far from the ruptured source. While there are different opinions regarding the near-fault zone location, the most common is restricted within a 20 km distance of the ruptured fault (Bray and Rodriguez-Marek, 2004). Baziar and Rostami (2017) mentioned that the near-fault region is limited by the magnitude of a seismic event that is equal to $R_t(km) = 0.3M_w^2$. Wave propagation effects or the so-called 'forward-directivity' (FD) affect near-fault sites. The fault rupture propagation toward a site at a speed that nears the shear wave velocity, oriented perpendicularly to the fault plane, form the FD effect (Somerville, 2003). Most seismic energy demands in FD pulses accumulate at the beginning of the record, which is evident in the large-period pulses in the velocity time history. It is worth noting that the ratio of seismic energy of directivity pulses to the energy of the whole earthquake in near-fault records can be up to 80%. This indicates the importance of near-fault excitations (Mukhopadhyay and Gupta, 2013).

Also, ground shaking in the near-fault zone, parallel to the fault strike with strike-slip mechanism or in the fault-normal direction for dip-slip faults may be affected by a permanent static movement called the 'fling-step' (Somerville et al., 1997). The FD effect is a dynamic phenomenon that does not leave permanent ground movements; as observed in the time history, FD produces two sided velocity pulses, while the fling-step, caused by permanent earth displacements, makes one-sided velocity pulses (Bray and Rodriguez-Marek, 2004).

All of the above explanations reveal that near-fault records are inherently different from larger site-to-source recorded shakings and, therefore, require special consideration when designing geotechnical and structural systems. Bertero was the first to report the devastating failure capacities of near-source earthquakes (Bertero et al., 1978). The catastrophic earthquakes of the 1990s such as the Northridge (1994), Kobe (1994) and Chi-Chi (1999) earthquakes led to a wide range of research efforts, aimed at assessing the performance and damage potential of various geotechnical and structural systems subjected to near-fault pulse shakings (Hall et al., 1995; Alavi and Krawinkler, 2000; Garini and Gazetas, 2013; Davoodi et al., 2013).

Gazetas et al. (2009) presented a numerical study on a rigid block that was supported by a frictional contact surface and charged by motions having forward-directivity or fling-step effects. They concluded

* Corresponding author.
E-mail addresses: m_aghamolaei@civileng.iust.ac.ir (M. Aghamolaei), asaeedia@iust.ac.ir (A. Saeedi Azizkandi), Baziar@iust.ac.ir (M.H. Baziar), s_ghavamijamal@civileng.iust.ac.ir (S. Ghavami).

https://doi.org/10.1016/j.compgeo.2020.103924
Received 12 March 2020; Received in revised form 10 November 2020; Accepted 13 November 2020
Available online 3 December 2020
0266-352X/

Notations

PGA	Peak ground acceleration
FD	Forward directivity
FE	Finite element
Mw	Magnitude of earthquake
M-O	Mononobe–Okabe
PGV	Peak ground velocity
ω	Natural frequencies
μ	Frictional coefficient
v_s	Shear wave velocity
v_p	Body wave velocity
ρ	Bulk mass density
PPV	Peak to peak velocity
σ	Stress
ε	Shear strain
G	Shear modulus
f	Frequency
υ	Poisson ratio
ϕ	Friction angle
C	Soil cohesion
Ψ	Dilation angle of the soil
γ	Unit weight
Tp	Predominant period

that the upper-bound sliding displacements from near-source excitations may substantially exceed the values obtained from some of the currently available design charts. Song and Rodriguez-Marek (2014) developed a coupled method for analyzing the sliding-blocks of slopes under near-fault pulse-like and nonpulse-like ground motions. The authors found that the slope is expected to experience larger displacements when near-fault ground motions have pulse-like characteristics. Zou et al. (2017) conducted a numerical analysis and found that the seismic response of concrete face rockfill dams increased with an increasing ratio of the peak ground velocity to the peak ground acceleration (PGV/PGA). Higher values of crest displacement as well as intense damages to the concrete face were among the consequences of near-fault shakings.

It is evident from the literature that near-fault ground motions are susceptible to inducing large displacements on different types of geotechnical structures. Hence, the role of these types of excitations is crucial to consider when designing by performance-based procedures. Retaining walls are an example of a one such system and are widely used for stabilizing excavations in roads and highways, especially for urban areas. Extensive applications lead to constructing retaining structures in seismic regions and areas that are close to active faults. The seismic response of retaining walls is a complicated problem because it involves dynamic soil-structure interactions. Seismically induced lateral displacements, dynamic bending moments and pressures behind the retaining structures are multi-dimensional problems that depend on wall foundation and backfill soil, the inertial and rigidity of the wall itself, and the nature of input excitations.

The classic methods proposed by Okabe (1924) and Mononobe and Matsuo (1929), known as the Mononobe–Okabe (M-O) as later developed by Seed (1970), are still the main approaches for the design of retaining walls. This method recruits the pseudo-static equilibrium by simplifying earthquake loading as an inertial force, without considering the dynamic characteristics of input earthquake loads and retaining walls. Since then, various researches have been conducted to assess the seismic performance of retaining walls by means of experimental (Nakamura, 2006; Kloukinas et al., 2014; Jo et al., 2017; Candia et al., 2016); numerical and analytical approaches (Veletsos and Younan, 1997; Psarropoulos et al., 2005; Nimbalkar and Choudhury, 2007; di Santolo and Scotto and Aldo Evangelista., 2011; Brandenberg et al., 2017; Bakr et al., 2019).

Gazetas et al. (2004) used finite-element modeling to explore the magnitude and distribution of dynamic earth pressure forces on several types of flexible retaining systems. By using dynamic centrifuge experiments performed on cantilever walls and following two-dimensional nonlinear finite-element analysis, Atik and Sitar (2010) concluded that the current design methods based on the M-O theory significantly overestimated the captured dynamic earth pressure forces and moments and mentioned that seismic earth pressures along with cantilever retaining walls can be neglected at accelerations below 0.4 g. By focusing on displacements, Conti et al. (2012) showed that maximum accelerations smaller than the critical limit equilibrium value increase the structural loads, thereby, subjecting the retaining walls to significant permanent displacements. Cakir (2013) analyzed the effect of earthquake frequency content on the seismic response of retaining structures and reported that wall responses are highly dependent on the PGV/PGA ratio and can cause a spiked increase or decrease in system displacement by the frequency content variation. Bakr and Ahmad (2018) developed charts and correlated between seismic earth pressure and wall movement. The authors reported that accelerations greater than 0.4g enabled the retaining wall to continue moving without enhancing the dynamic passive earth pressure forces. Mikola et al. (2016) recorded distribution of the seismic earth pressures on cantilever retaining structures using centrifuge tests. Salem et al. (2020) performed a series of two-dimensional finite element methods for analyzing the seismic response of cantilever retaining walls. The sensibility of the system response to the soil constitutive model was studied. A Rigid perfectly plastic (M-C) and an advanced nonlinear elastoplastic model (HSSMALL) were used. The results of the analysis showed that in the M-C model, a larger force than HSSMALL was captured. Furthermore, a higher value of lateral displacement for the 1989 Loma Prieta-UCSC earthquake was recorded in the M-C model. Conti and Caputo (2019) investigated the dynamic response and phase shift between soil and the inertia forces under a real earthquake. Jadhav and Prashant (2020) proposed displacement-based design procedures for cantilever retaining walls. The authors reported that using shear key placed at the heel of cantilever retaining wall was reduced the transitional displacement by 40%. Santhoshkumar et al. (2019) investigated the earth pressure behind cantilever retaining walls using a pseudo-dynamic approach. Zamiran and Osouli (2018) correlated the free-filed PGA to the relative displacement of the wall under real earthquakes. They reported that 50% of walls experienced failure state when input PGA reached to 0.47g for cohesionless backfill.

Reviewing the literature shows that most dynamic studies on retaining walls are limited to the earth pressures and forces that act along with the structures. The number of displacement-based studies of retaining walls is rare. Also, the performance of cantilever retaining walls under near-fault excitations is not yet well understood. The conformity of seismic wall movements in real earthquake scenarios with failures and permissible states are also unknown. So, further research about response and seismic forces behind retaining walls that are motivated by near source motions are needed. Qualitative insight into the performance analysis of retaining walls under near-fault strong ground motions will emphasis on the importance of displacement-based designs.

In this regard, the present research evaluated the results of a series of dynamic 2D finite element (FE) numerical models based on the performance of cantilever retaining structures under near-fault excitations with a focus on seismically induced lateral displacements. Due to the higher damage potential of FD over fling step (Bray and Rodriguez-Marek, 2004; Kalkan and Kunnath, 2006), this research was mainly focused on FD shakings and used fully dynamic time-domain analyses in the process. In the first section and to illustrate the importance of the

discrepancies in wall responses under near and far-field ground motions, FD pulses were extracted from the velocity time series of near-fault, main, and residual records and imposed on the verified model. Then, near-fault strong ground motions with a wide range of PGAs from 0.1 g to 0.6 g were applied for different shaking scenarios. The captured movements were compared with the recommended criteria for the performance-based aseismic design of soil retaining structures in the literature. A comprehensive parametric study was applied to assess the effect of different parameters. The effect of the mechanical properties of backfill/foundation soil as well as the frequency content of the ground motion was investigated.

2. Methodology

Selecting near-fault ground shakings beside the far-field records, as subdivided into pulse-like and non-pulse ground motions, and comparing the structure responses under these types of seismic loads are common procedures widely applied in the literature. This study employs a novel approach called the wavelet analysis. The wavelet approach is a signal processing procedure that decomposes signals such as seismic ground motions (Baker, 2007). Many researchers have evaluated the wavelet analysis for the characterization of near-source earthquakes (Mavroeidis and Papageorgiou, 2003; Mollaioli and Bosi, 2012; Vassiliou and Makris, 2011).

Baker (2007) developed a wavelet based transform for records with PGV $>$ 30 cm/sec which are classified as pulse-like ground motions. In this research, near-fault records containing forward directivity were compiled from a database developed by Baker (2007) and Hayden et al. (2014), which was obtained from the Pacific Earthquake Engineering Research Center website (PEER). Table 1 presents a brief summary of the near-fault ground motion properties used in this research.

After selecting the near-fault earthquake ground motions, the extracted pulses from the velocity–time history were subtracted from the main records, and new excitations indicating far-field earthquakes were created. An example of the extracted pulse from the primary record is depicted in Fig. 1.

Contrary to the common procedure used in the literature, these semi-artificial earthquakes act precisely like the main ground motion, except that they occur in the range of pulse time, manifesting just the effect of the forward directivity pulse. Fig. 2 shows the acceleration, velocity and displacement time series of the main record and the generated far-field record from the Landers earthquake in 1992 at the Lucerne station. A comprehensive database of different magnitudes, durations and peak value of velocities was considered for assessing the effect of the directivity pulse on the seismic response of cantilever retaining walls (Table1).

As mentioned above, it is obvious that all characteristics of the two records are the same, except in the pulse acting domain. A comparison of Fig. 2a and b shows that eliminating the directivity pulse decreased the peak ground velocity by about 50%; whereas decreased the maximum magnitude of acceleration by only 10%. To further elaborate, the ratio of peak ground velocity to peak ground acceleration (PGV/PGA) went from 0.18 s in the main record to 0.1 s in the generated motion, indicating the importance of the directivity pulse.

Table 1
near-fault ground motions database considered in this study investigation.

Event	Station	PGV (cm/s)	Rrup (km)	PGV/PGA (s)	Arias intensity (m/s)	Tp (s)
Imperial Valley-06	El Centro - Meloland Geot. Array	92.6	0.07	0.302	1.105	0.56
Kobe, Japan	Takarazuka	86.3	0.27	0.143	3.935	0.48
Morgan Hill	Coyote Lake Dam	78.3	0.53	0.061	3.855	0.3
Parkfield-02, CA	Parkfield-Cholame 2WA	63.9	3.01	0.104	1.643	0.66
San Fernando	Pacoima Dam (upper left abut)	114.47	1.81	0.096	8.948	0.38
Tabas, Iran	Tabas	123	2.05	0.146	11.808	0.2
Loma Prieta	LGPC	96	3.8	0.172	7.194	0.7
Landers	Lucerne	133.5	2.19	0.188	6.972	0.08
Northridge-01	Pacoima Dam (upper left)	103.6	7.01	0.082	8.596	0.16
Chi-Chi, Taiwan	TCU102	91.65	1.5	0.307	2.025	0.72
Landers	Yermo Fire Station	151.33	23.6	0.213	8.089	0.68
Bam, Iran	Bam	124	1.7	0.157	8.019	0.2

3. Numerical modelling and calibration

The two–dimensional plane strain dynamic implicit method is applied for the numerical analyses of a cantilever retaining wall using the ABAQUS finite element based software (2014). The shaking table test results obtained by Kloukinas et al. (Kloukinas et al., 2014, 2015) were simulated in the prototype scale to calibrate the results of the numerical modeling.

3.1. Model geometry

The experimental tests conducted by Kloukinas et al. (2014, 2015) and used for numerical validation were performed in a large Equivalent Shear Beam container of EQUALS, with inner dimensions of 4.80 m long, 1 m wide and 1.15 m deep. A maximum soil height of 1 m was selected, corresponding to a wall height of 0.6 m and a foundation soil layer of 0.4 m. A frequency scale magnitude equal to 5 was considered for the model/prototype of this research. The dynamic time and frequency for 1 g shaking table tests should be scaled in the prototype to satisfy the compatibility between gravity and inertia forces (Iai et al., 2005). The simulation law for 1 g shaking table tests, proposed by Iai et al. (2005), was applied and resulted in a prototype to model the scale factor of 8.5 ($N = 8.5$). An 8.5 m height was, therefore, modeled for the prototype soil layer. A backfill of 5.1 m and a foundation layer of 3.4 m were simulated in the prototype scale. The length of the wall was equal to the backfill layer. Hence, a wall height of 5.1 m and a thickness of 0.25 m were modeled in the numerical simulation.

The scaling factors for different parameters used in the numerical model are presented in Table 2.

The soil body was modeled with structured triangle six-noded elements (CPE6) due to the geometrical nonlinearity of the system. The wall was modeled with the same element and a refined size. The sensibility analysis of different mesh sizes was used to select the best mesh dimensions, satisfying both accuracy and time of analysis. A dimension of 0.2 m * 0.3 m was selected for the region next to the wall, and the mesh sizes were larger at the soil boundaries. Finer element size will increase runtime with no significant change in results.

3.2. Soil properties and the constitutive model

The elastic perfectly plastic soil model with a Mohr-Coulomb (M-C) plastic failure criterion and isotropic softening was applied as a constitutive model for the soil body. Softening is implemented by the reduction of friction and dilatation angle referred to (Anastasopoulos et al., 2007).

Despite the simplicity, the M-C model is the most common model used in numerical programs for modeling the soil behavior (Salem et al., 2020). This model was widely utilized for modeling the response of cantilever retaining walls subjected to seismic motions in previous contributions (Green et al., 2008; Madabhushi and Zeng, 2007). This soil model was used even with software that was capable to apply advance models like FLAC software (Conti and Caputo, 2019). Salem et al. (2020)

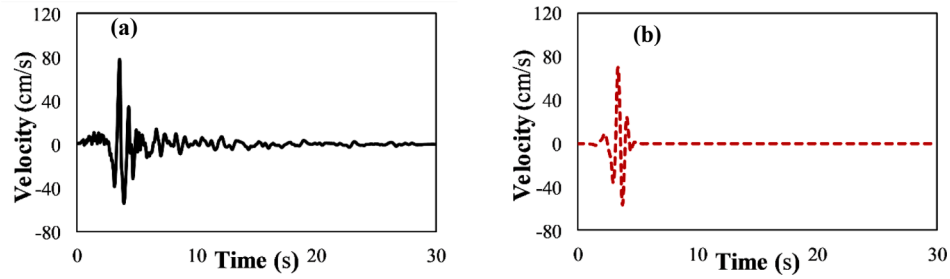

Fig. 1. Morgan hill velocity time history recorded during shaking at Coyote Lake Dam: (a) Main near-fault record; (b) Extracted pulse.

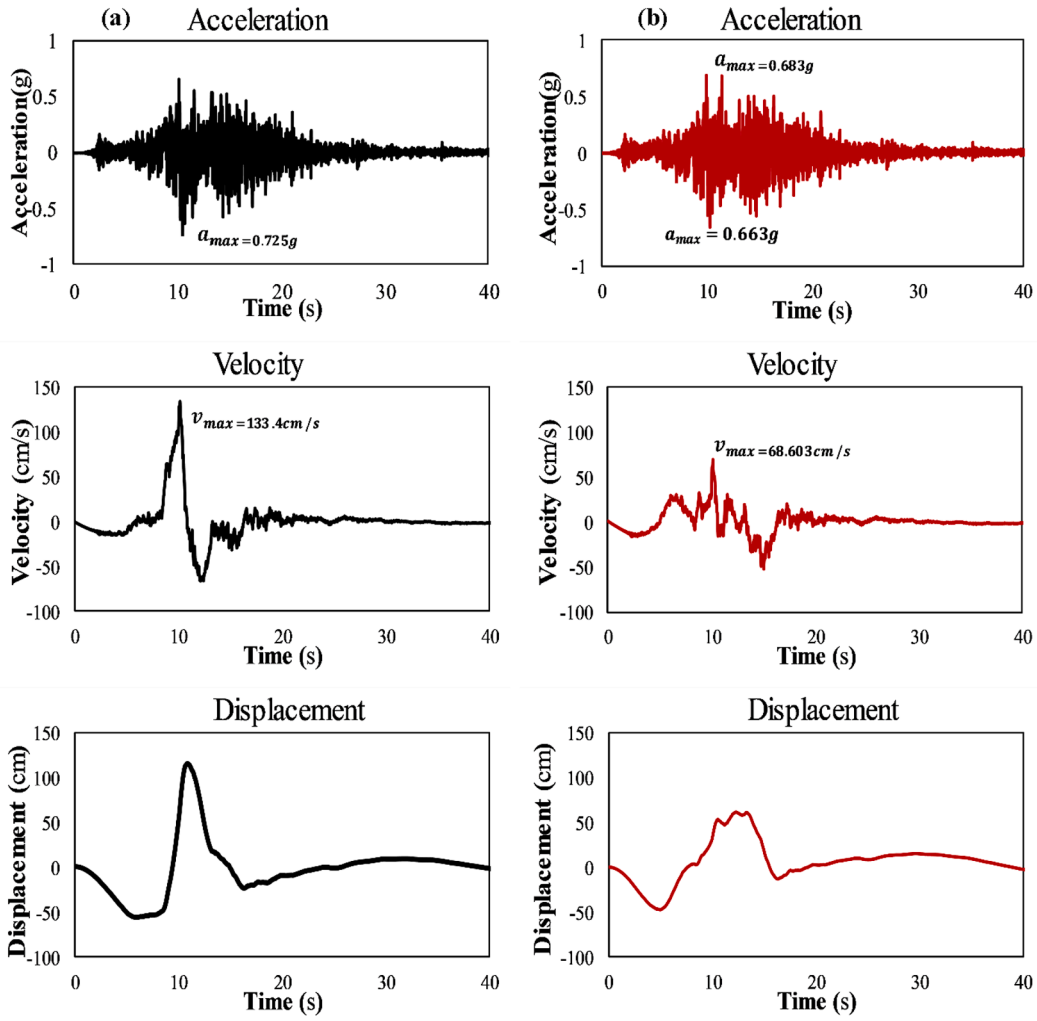

Fig. 2. Landers time histories recorded during shaking at Lucerne station: (a) Main near-fault record; (b) Generated far field record.

used Plaxis software and M-C and HSSMALL models. Based on (Salem et al., 2020) results, it can be concluded that although M-C constitutive model is a simple model but predicts the performance of cantilever retaining wall with an acceptable degree of accuracy especially in case of displacement studies. Furthermore, the finding of authors revealed that using the M-C model may be conservative due to the prediction of higher values of forces and displacement. Base on the mentioned statement using M-C is an appropriate model for addressing seismic lateral displacement of cantilever retaining wall under real earthquake scenarios and initial investigation for addressing current study.

It should be noted that despite the wide application of the M-C model, many aspects of soil may not be modeled as real. However, the fundamental findings and basic concepts of this research can be useful for future interests.

Both the backfill and foundation soil layers were dry sand with different compaction levels. An un-cemented sand (yellow Leighton Buzzard 14–25 (Fraction B) silica sand) with 60% relative density of a foundation layer and 22% for a backfill with dense and medium dense layers, respectively, were used in the experimental tests. The peak values of friction angle for backfill and foundation are reported as 33.5° and 42.5° by Kloukinas et al (Kloukinas et al., 2014; di Santolo and Aldo, 2011), respectively. The numerical results are calibrated by using sensitivity analysis of the friction angles of backfill and foundation soils to be matched with the shaking table test results. The best compatibility in the case of lateral displacement between numerical modeling and the experimental test is achieved when the peak friction angles of

Table 2
Scaling factor for 1 g shaking table tests.

Item	Sign	Prototype/model	This research
			P/M
Density	ρ	1	1
Length	L	N	8.5
Stress	σ	N	8.5
Shear strain	ε	$N^{0.5}$	2.9
Displacement	d	$N^{1.5}$	24.7
Shear modulus	G	$N^{0.5}$	2.9
Acceleration	a	1	1
Frequency	f	$N^{-0.75}$	0.2
Dynamic time	t	$N^{0.75}$	5

foundation and backfill in the FEM model are reduced to 39° and 30°, respectively. The calibrated soil properties used in the numerical model are summarized in Table 3.

The damping ratio was defined in the model via two Rayleigh damping coefficients, α and β. The coefficients determine the damping matrix C, which is a function of the mass and stiffness matrices, see Eq. (1).

$$C = \alpha M + \beta K \tag{1}$$

The two Rayleigh damping coefficients α and β were determined using Eqs. (2a) and (2b), as developed by Ju and Ni (2007):

$$\alpha = 2\omega_1\omega_2(D_1\omega_2 - D_2\omega_1)/(\omega_2{}^2 - \omega_1{}^2) \tag{2a}$$

$$\beta = 2(D_2\omega_2 - D_1\omega_1)/[\pi(\omega_2{}^2 - \omega_1{}^2)] \tag{2b}$$

where D_1 and D_2 are fractions of critical damping at two different circular natural frequencies (ω_1 and ω_2).

The retaining wall was modeled as a non-yielding element in experimental procedures by using aluminum material. Because the wall behavior is fully linear elastic and perfectly rigid, damage potential and flexibility were not defined in the numerical model. The aluminum wall in the experimental tests was modeled using the reinforced concrete material in the prototype simulating the real type of cantilever retaining walls. Also, a rough interface between wall and soil was created in the experimental tests by pasting rough sandpaper on the footing surface (Kloukinas et al., 2014, 2015). This rough contact simulated the real concrete-soil interface, and the assumption made regarding the concrete retaining wall was logical.

3.3. Soil wall interaction and boundary condition

The contact type interaction was used to appropriately model the interface between soil and wall. The tension-less but frictional behavior was simulated by the defining μ coefficient for tangential behavior. An interface friction angle of 28.5° was obtained from the static pull out test by Kloukinas et al. (2015). The normal behavior and the hard contact was applied to allow both separation and sliding,

To reduce the radiation damping effect, Lysmer and Kuhlemeyer (1969) and Kuhlemeyer and Lysmer (1973) proposed applying viscous boundary conditions to absorb reflected waves along the artificial boundary. In order to capture the effects of box and wave reflection into the model, two vertical free-field soil columns were defined and connected each side of the model to the main part using normal and shear viscous dashpots, representing the viscous boundary condition. Coefficients of the dashpots were ρv_s and ρv_p per unit area; where ρ is the density of the material and v_s and v_p are the s-wave and p-wave speed, respectively. Dashpots absorb energy in a procedure similar to that used in the application of quiet boundaries. Dashpots make viscous normal and shear tractions. The mesh generated pattern as well as artificial soil columns and viscous boundaries are depicted in Fig. 3.

Table 3
Soil properties used in validation.

Item	G (MPa)	Poisson ratio (υ)	φ_p (°)	φ_{res} (°)	ψ_p (°)	ψ_{res} (°)	γ (KN/m^3)
Backfill soil	58	0.3	30	30	0	0	15.1
Foundation soil	116	0.3	39	36	9	6	16.1

3.4. Calibration

Numerical modeling was applied to simulate shaking table experiments based on a prototype wall. Seismic sinusoidal excitation was, therefore, used in the experimental program and scaled to the time and frequency domain, with the same amplitude of 0.23 g and rough interface configuration of the experimental program. The top wall seismic displacement, accelerations in both the bottom and top of the wall, and dynamic bending moment along the wall were all validated. Fig. 4 shows the numerical and experimental results of FE and the experimental models. Based on the results, it can be concluded that the proposed numerical model matched the physical modeling results with a reasonable degree of accuracy. The difference found in the range of lateral displacement in the numerical and physical model is mainly due to the fact that in the FE model, relative displacement between the wall and displacement time history of loading is captured and is not a pure movement of the soil and structure system. In this condition, both the wall and motion displacement time series have a similar oscillation and different absolute values. Using relative displacement eliminates the oscillation domain and captures the residual displacement in the wall. Based on the aforementioned explanations and despite the incompatibility found in oscillations of the upper and lower bands of displacements, it can be concluded that the total residual movement is fitted with a good degree of accuracy as marked in Fig. 4 a.. Garini et al., on the other hand, reported a similar trend of bending moments along the wall, as modeled by the FE method (Garini et al., 2016).

Following model validation through imposing earthquake motions (near-fault and semi-artificial far-field records) to the base of the model in X direction, the soil-structure response was captured and reported in the present research.

4. Response of the cantilever retaining wall to near-fault motions

To better understand the impact of near-fault earthquakes, the results of two famous events with medium and high PGA values, specifically the Landers earthquake, recorded at the Lucerne station, with a PGA equal to 0.725 g and the Chi-Chi event, recorded at the TCU102 station, with a PGA equal to 0.3 g, are compared and presented in this section. The acceleration and velocity time histories of the TCU102 record are depicted in Fig. 5.

4.1. Top wall displacement and settlement

The displacement and settlement time histories of the Landers earthquake at the Lucerne station and the Chi-Chi earthquake at the TCU102 station along the highest point of the wall are depicted in Fig. 6a and 6b, respectively.

It can be concluded from the results that about 47% and 39% of the final residual displacements and settlements caused by earthquake loading occurred in a narrow band of 2 s, which is mainly due to the directivity pulse of the Landers and Chi-Chi earthquakes, respectively. This finding is in complete agreement with the fact that the main part of seismic demand in pulse-like motions is accumulated in the directivity pulse (Mukhopadhyay and Gupta, 2013). Eliminating the pulse from the

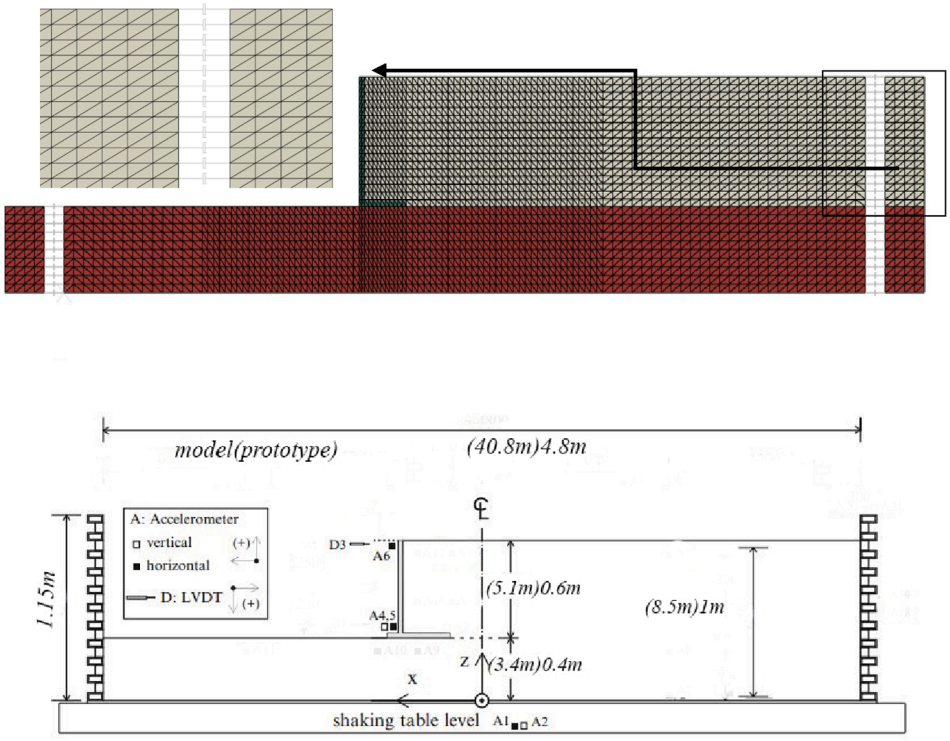

Fig. 3. Cantilever retaining system a) Numerical model b) experimental configuration (Kloukinas et al., 2015).

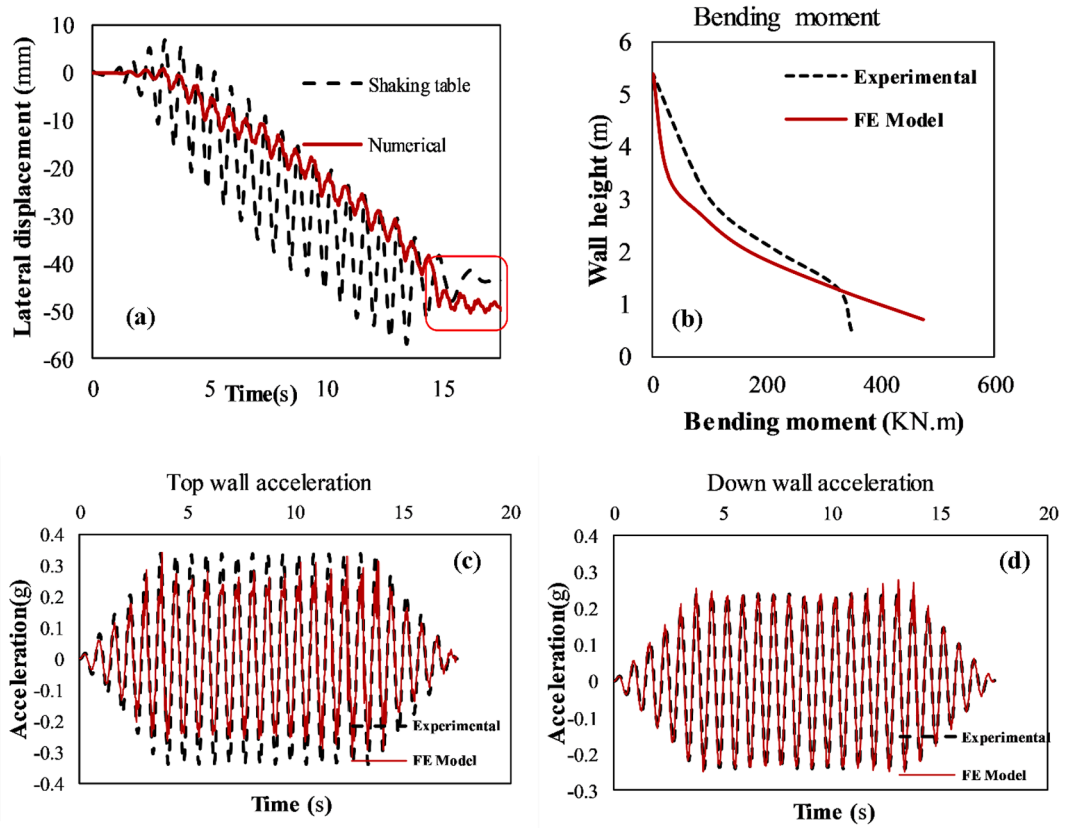

Fig. 4. Comparison between the numerical prediction and experimental results.

main records helped reduce the final residual displacements imposed by these earthquakes. As previously mentioned, while the maximum acceleration of the generated far-field motion in the main records was only slightly reduced, prominent differences captured in the displacement showed the vital role of the velocity time history. The effect of forward directivity on the performance-based design of retaining structures, as

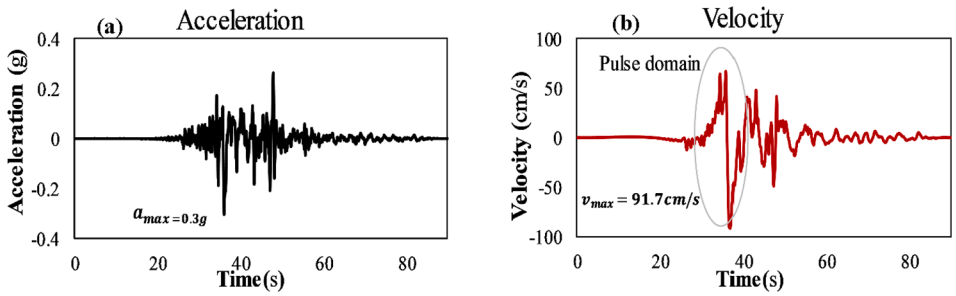

Fig. 5. Chi-Chi time histories recorded during shaking at TCU102 station: (a) Acceleration; (b) Velocity.

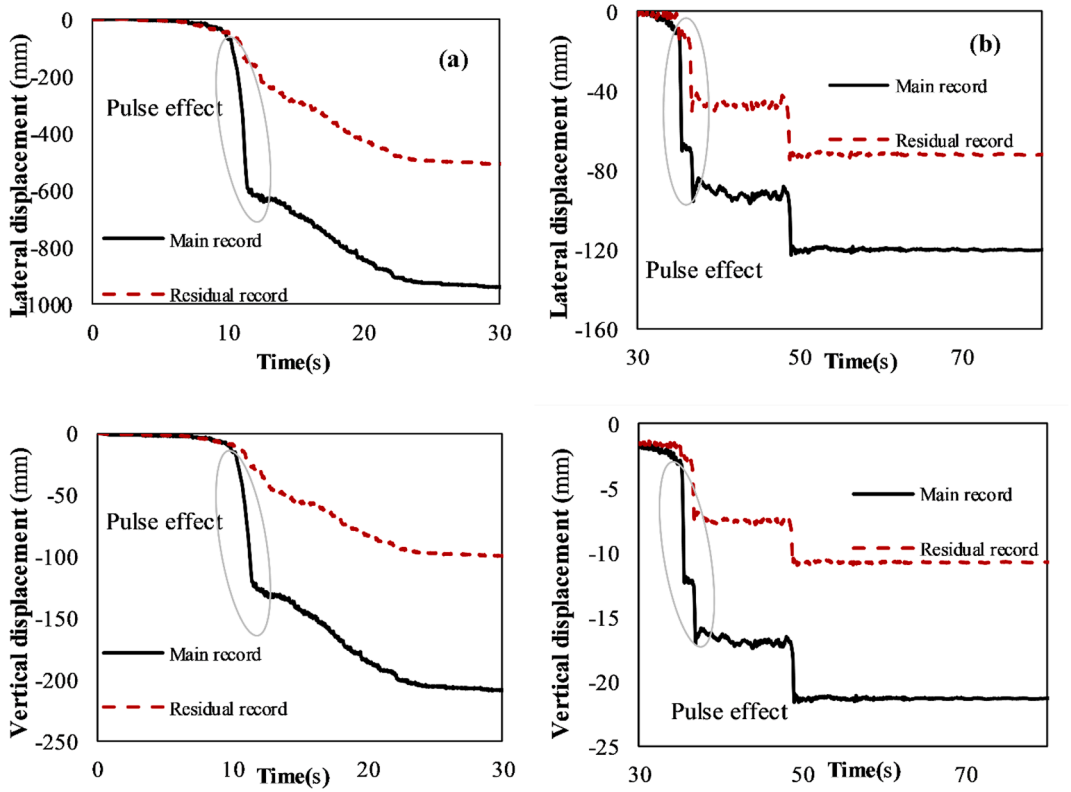

Fig. 6. Top wall displacement and settlement time histories of main and generated far field record for earthquake (a) Landers; (b) Chi-Chi.

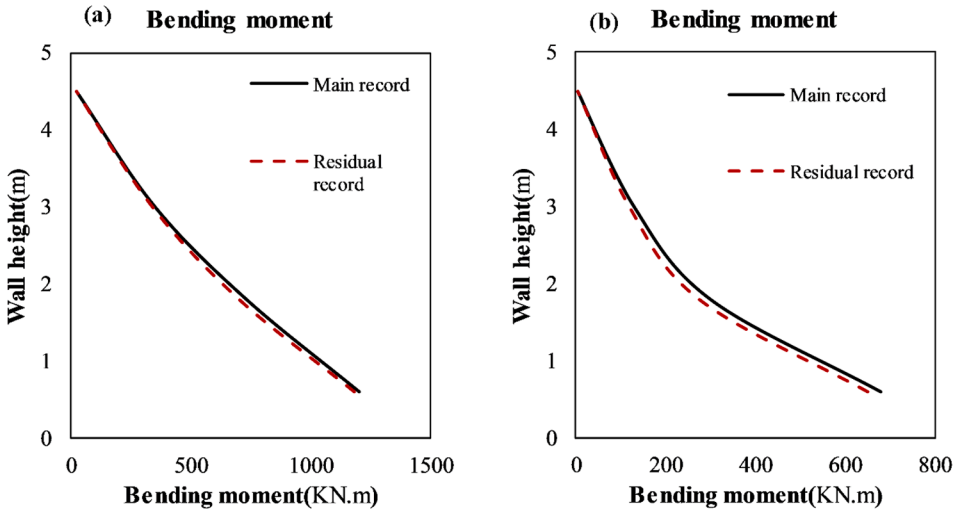

Fig. 7. Bending moments of main and generated far field record for earthquakes: (a) Landers; (b) Chi-Chi.

illustrated by the results of the movements mentioned herein, is also important to consider.

4.2. Bending moment along the wall

The effect of near-fault ground motions on the distribution of forces along the wall and bending moment in the height of the wall should be considered. Results of the bending moment induced by the Landers (Lucerne) and Chi-Chi (TCU102 station) excitations are illustrated in Fig. 7.

It can be concluded that having approximately the same PGA but different PGV can still provide equal distribution of bending moment along the wall. Besides the apparent discrepancy in the lateral displacements of the wall, these results illustrated the inherent differences of the earthquakes recorded in the vicinity of the ruptured faults. These observations are compatible with the findings of Bakr and Ahmad (2018). The authors noted that seismic active earth pressures were not dependent on wall lateral displacements during a shaking. As mentioned before, eliminating the pulse from the main shocking slightly decreases the PGA of input motion, causing the bending moment of the wall in the near-fault and far-field scenarios to experience almost the same seismic forces. The accuracy of the findings can be justified with these facts.

4.3. Effect of velocity and acceleration

Fig. 8 compares the magnitude of a peak to peak velocity (PPV) and the peak ground acceleration of records reported in Table 3 with the captured responses of the numerical modeling.

As seen in Fig. 8a, the absence of a clear relationship between the magnitude of acceleration and induced lateral displacement led to a vast data scatter. However, as seen in Fig. 8b, using PPV instead of PGA made the chart more regular and trend-line has been manifested. Davoodi et al. (2013) reported a similar trend for an embankment dam that was excited by near fault records. Zamiran and Osouli (2018) developed an equation and connected the maximum displacement of the cantilever wall to the PGA of free field. Findings of the current study showed that this equation is not accurate enough for the near-fault earthquake

The report on the close connection between velocity and displacement found velocity to be the main factor in the seismic analysis of retaining structures excited by pulse-like ground motions, a factor that had not been considered considerably in traditional approaches. While the same process was observed for PGV, the PPV trend-line reported in this research was found to be more accurate.

5. Performance-based analysis

A comparison of the results shows that the lateral displacement of the wall was remarkably higher under near-fault ground motions than far-field ground motions. This brings up the concern that perhaps near-fault type of motion imposes a larger movement than the permissible and ultimate values of the displacements mentioned in the literature. Hence, a comprehensive study was employed by imposing different near-fault earthquake scenarios with PGAs ranging from 0.1 g to 0.6 g, to the verified model, and the results were compared with the criteria found in the literature and codes. Some of these criteria are reported in Table 4.

The results of the numerical model are depicted in Fig. 9 and reported in Table 5.

Table 5 and Fig. 9 show that the walls that fell into the range of low to moderate earthquakes (0.1–0.3 g) experienced lower horizontal displacements than permissible and the failure states have been noted in the literature. However, acceleration of 0.4 g induced a lateral displacement to the wall that was larger than the permissible state but failure condition did not occurred, yet. For base accelerations of more than 0.5 g the lateral movement of wall exceeded from the failure state reported by Huang et al. (2009). Fig. 10 illustrates the normalization of the data by dividing the Commission of the European Communities (The Commission of the European Communities European prestandard, 1994) values into the residual displacements captured from different events. As seen in Fig. 10; strong motions caused the retaining wall to experience a displacement of up to 5 times the recommended value. Under the assumptions made in this research, an acceleration of 0.4 g for near-fault records was the critical value that imposed devastating displacements onto the system and caused failure state. For validation of this fact, all scenarios with the seismic properties reported in Table 1 were compared with the permissible and failure states reported in Table 6. The data showed that 83% of ground motions in this study had a PGA greater than 0.4 g. It is noticeable that all the records sensed a displacement that was larger than the permissible state. According to the Huang et al. failure state protocol (Lysmer and Kuhlemeyer, 1969); 50% of motions experienced movement greater than 5% of the wall height. Based on the Wu and Prakash et al. failure limit (Wu and Prakash, 1996), 33% of cases experienced a larger lateral displacement than 10% of the wall height. The wall failure is reported when PGA of input motion reaches 0.47 g in 50% of cases (Zamiran and Osouli, 2018) which is close

Table 4
Criteria for performance-based analysis of retaining walls.

	Eurocode 8 The Commission of the European Communities (1994)	Wu and Prakash (1996)	AASHTO (2002)	Huang et al. (2009)
Permissible state(mm)	$300a_{max}$	0.02*H	$250a_{max}$	0.02*H
Failure state (mm)	–	0.1*H	–	0.05*H

a_{max} = maximumearthquakeacceleration(g)
H = Wallheight(mm)

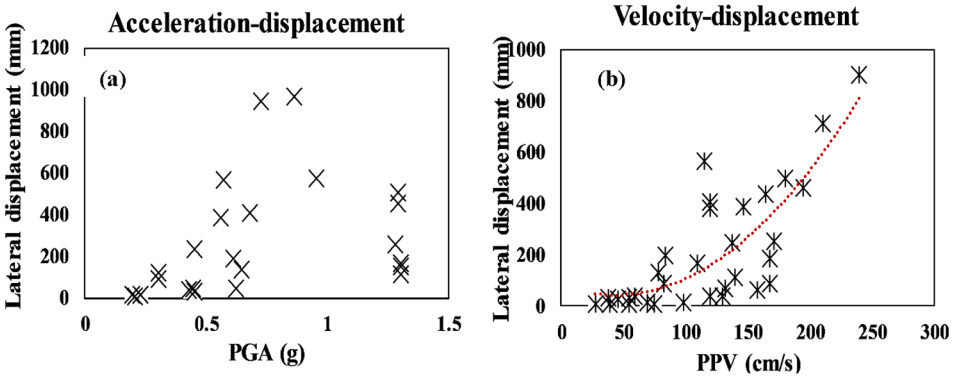

Fig. 8. Correlation between lateral displacement of wall and (a) PGA; (b) PPV.

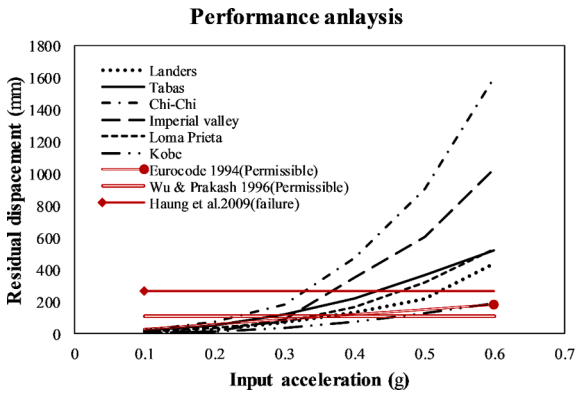

Fig. 9. Seimic displacement of wall under near-fault motions with performance-based criteria.

Table 5
Displacement of wall in different scenarios.

Acceleration (g) Event	0.1	0.2	0.3	0.4	0.5	0.6
Landers(Lucerne)	9.8	29.7	74.8	134.2	217.1	437.9
Imperial Valley-06(El Centro - Meloland Geot. Array)	4.8	16.8	92.8	351.4	606.5	1028.7
Kobe(Takarazuka)	9.7	16.2	37.6	78.8	129.4	198.6
Loma Prieta(LGPC) Landers	12.9	36.8	78.3	165.3	318.6	528.4
Tabas, Iran	20.3	55.5	123.7	223.2	366.0	523.8
Chi-Chi(TCU102)	19.8	73.2	182.1	476.1	908.1	1593.2
The Commission of the European Communities (1994)	30	60	90	120	150	180
Wu and Prakash (1996)	108	108	108	108	108	108
AASHTO (2002)	25	50	75	100	125	150
Huang et al. (2009)	108	108	108	108	108	108
Huang et al. (2009) (failure)	270	270	270	270	270	270

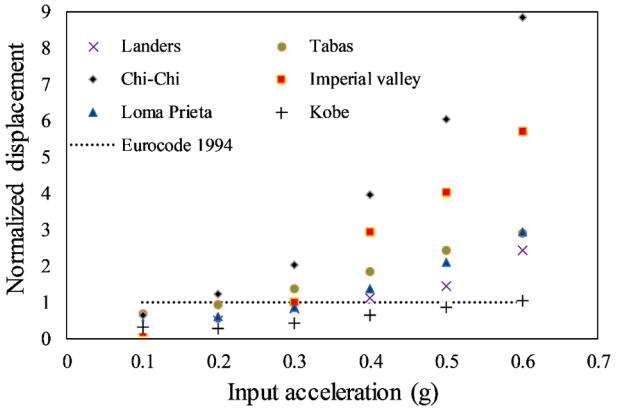

Fig. 10. Normalized Seimic displacement of wall under near-fault motions with Eurocode 1994.

to the results of current numerical models

These findings indicate that the absence of proper solutions in the design process of retaining structures for reducing displacements increases the failure states under near-fault ground shakings. Semi artificial motions generated in Section 2 were scaled with the same values of near-fault records, and responses of the wall were recorded to compare the results of near and far field records. For better comparison, only records with a single obvious pulse in the velocity time series were selected. As seen in Fig. 11, far field scenarios cause smaller displacements and have lower failure states in all cases, except at an acceleration of 0.6 g. These findings again confirm the importance of near-fault excitations and show that basing a decision on only the base acceleration may cause catastrophic consequences.

On the other hand, certain instructions, including the EN 1998–5 procedure, tend to underestimate the residual displacements and cannot predict failure (Deyanova et al., 2016). The above statements show that the displacement analysis of retaining walls is a complicated problem that needs precise approaches in high seismic hazard sites.

6. Parametric study

The verified FE model was used on a prototype scale to examine the effect of various parameters, such as the magnitude of input acceleration, geotechnical properties of backfill and foundation soil as well as the frequency content of the main shocking on seismic responses of the retaining structure.

6.1. Magnitude of input acceleration

As illustrated in Fig. 12, the different absolute values of the input acceleration of the Loma Prieta earthquake at the LGPC station, which ranged between 0.1 g and 0.57 g (the PGA of main records), were applied.

As seen in Fig. 12, all parameters were kept at a constant value, and the effects of the acceleration magnitude were recorded. Fig. 12a and 12b show that increasing the acceleration strongly changes the lateral and vertical displacements of the top wall. The figures also show the effect of directivity pulses on wall displacement. It is worth noting that scaling the acceleration magnitude kept the PGV/PGA ratio the same in all models. The results show that increasing the acceleration magnitude also increases the displacement and, thereby, worsens the condition of the settlements. The bending moment along the wall is shown in Fig. 12c. The more the acceleration values of the wall, the greater the magnitude of the bending moments. Fig. 13 shows that aligning the lateral displacement and bending moment magnitudes with the acceleration values identified a distinctive trend, whereby, enhancing the input values led to further refining of the bending moment.

Lateral displacement of the acceleration value had a trend-line with a polynomial equation (order of 2). This is due to the seismic demand imposed on the models. The seismic energy of an earthquake, as widely discussed in the literature, is proportional to the square of velocity ($\int v^2 dt$). A trend-line with an equation of order 2 and a downward concavity was observed for the moment-acceleration chart, which indicates that increasing the acceleration reduces the rate of the moment enhancing. This is contrary to the results found in the displacement-acceleration charts. At an acceleration level greater than 0.4 g, the retaining wall was observed to move without increments in the seismic forces (Bakr and Ahmad, 2018). This finding is in good agreement with the results.

Another parameter measured against the acceleration magnitudes was the amplification patterns along the soil profile (Fig. 12d). Increasing the input motion value changes the value and amplification factor of the soil . The amplification factor was seen to decrease under higher level of excitations . This finding can be justified by the theory that suggests higher amplification values can be captured in lower levels of acceleration.

6.2. Properties of backfill soil

The response and performance of the retaining wall was examined against the geotechnical properties of the backfill layer by a comprehensive sensitivity analysis. The Loma Prieta earthquake at the LGPC station with PGA equal to 0.57 g is used as input motion in Sections 6.2 and 6.3. Fig. 14 illustrates the cohesion and friction angle.

The mechanical properties of the backfill soil had a considerable

Table 6
Displacement of wall at different scenarios for site acceleration.

Event	Station	Residual displacement (mm)	Permissible state	Huang et al. (2009)	Wu and Prakash (1996)
Imperial Valley-06	El Centro - Meloland Geot. Array	90.0	108	270	540
Kobe, Japan	Takarazuka	198.8	108	270	540
Morgan Hill	Coyote Lake Dam	144.2	108	270	540
Parkfield-02, CA	Parkfield-Cholame 2WA	58.6	108	270	540
San Fernando	Pacoima Dam (upper left abut)	595.9	108	270	540
Tabas, Iran	Tabas	1340.3	108	270	540
Loma Prieta	LGPC	466.9	108	270	540
Landers	Lucerne	941.2	108	270	540
Northridge-01	Pacoima Dam (upper left)	333.5	108	270	540
Chi-Chi, Taiwan	TCU102	122.6	108	270	540
Landers	Yermo Fire Station	826.3	108	270	540
Bam, Iran	Bam	1138.8	108	270	540

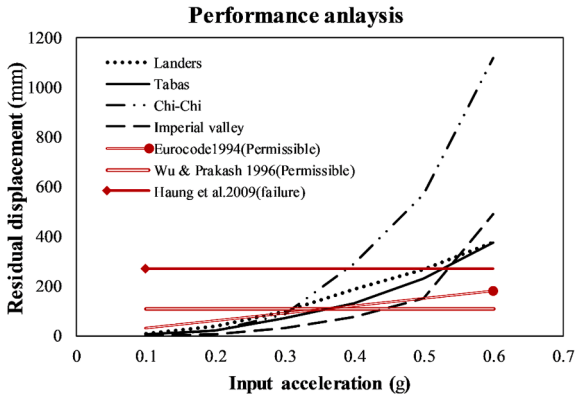

Fig. 11. Seimic displacement of wall under far field motions with performance-based criteria.

effect on displacement-based performances of the retaining structures. Improvements in the mechanical resistance properties of the backfill improved wall performance and reduced wall displacement. Enhancing the cohesion and friction angle did not significantly impact the distribution of the bending moment along the wall height, with variation of friction angle showing the least effect

. Increasing the magnitude of soil cohesion reduced the maximum bending moment value. A similar conclusion was reported by Osouli and Zamiran (2017). Their results showed that compaction of soil with a more significant relative density without changing the fine content improved the responses of soil-retaining structure systems. Furthermore, Zamiran and Osouli (2018) reported that Maximum lateral displacement of the wall with the cohesion of 10 kPa was a quarter of the displacement of cases with 0 kPa of cohesion. This statement is compatible with the results of Fig. 14.

6.3. Properties of the foundation soil

By using the findings of Section 6.2, the friction angle of foundation soil was changed to assess its impact on the system's response. Results of the displacements are depicted in Fig. 15. The lateral movement of the wall had a direct correlation with the friction angle. Changing the friction angles from 39 to 33 and from 39 to 45 changed the magnitude of the residual displacement by 49% and −26%, respectively.

It should be noted that the modulus of elasticity was constant in all models and the effect of the different magnitudes wasn't investigated in this work. Cakir (2014) performed a sensitivity analysis based on modulus magnitudes. It can be concluded from the results that lower values of displacements were captured in case of higher modulus.

6.4. Effect of the frequency content

One of the important aspects of the dynamic analysis of soil-retaining-structure systems is the frequency content of the input motion, which wasn't considered in more ordinary methods, such as the pseudo-static and M-O approaches. For assessing the effect of the frequency content on the seismic performance of the cantilever retaining walls, a series of input motions from distinct stations scaled in the same PGA imposed on the models and wall responses were captured. A similar method was employed by Cakir (2013), with the difference that the author used different earthquakes scaled to the same amplitude. Using different earthquakes for this purpose may not, however, only introduce the frequency content because the records have different faulting mechanisms and site conditions. For better comparison, motions of the same earthquake events recorded at different stations were used for evaluating the frequency content. The input motion of "Imperial Valley-06″ was selected, and the results are reported herein. All ground motions were in the vicinity of the fault rupture, representative of the same condition and scaled to the PGA of 0.3 g. The main properties of the selected station are reported in Table 7, and the Fourier spectrum of this motion is illustrated in Fig. 16.

The residual displacement and bending moment results of the frequency content effect are depicted in Fig. 17.

As seen in the figure, the maximum bending moment value in the record by the record with RSN number 171 was at a minimum among three records, but this motion imposed the highest residual displacement value into the wall. As reported in Table 7, this record contains a directivity pulse and PGV value. Given that the distribution of bending moments along the wall and the PGA were the same in the other two records, it can be concluded that increasing the PGV/PGA ratio, reported in Table7, increased the values of the lateral displacements of the wall. Cakir (2013), Bakr and Ahmad (2018) also discussed the effects of PGV/PGA ratios on wall response. So, the effects and main role of the frequency content of the ground motions are manifested in the response of the retaining structures, herein.

7. Conclusion

A series of dynamic finite element numerical models were conducted in the present research to evaluate the performance of cantilever retaining walls. Addressing seismically induced lateral displacements under near-fault excitations were the main part of interest. Due to the fact that forward directivity effect is more destructive than other near-fault effects, this paper concentrated on FD motions using a fully dynamic time-domain analysis. The wall bending moments, top horizontal displacement and settlements were measured as an index of the dynamic response of cantilever retaining walls. The captured lateral movements in a wide range of PGAs were compared with criteria that developed in literature and codes, for the permissible and failure states of wall displacement. A comprehensive parametric study was applied and effects of different parameters on the response retaining wall were

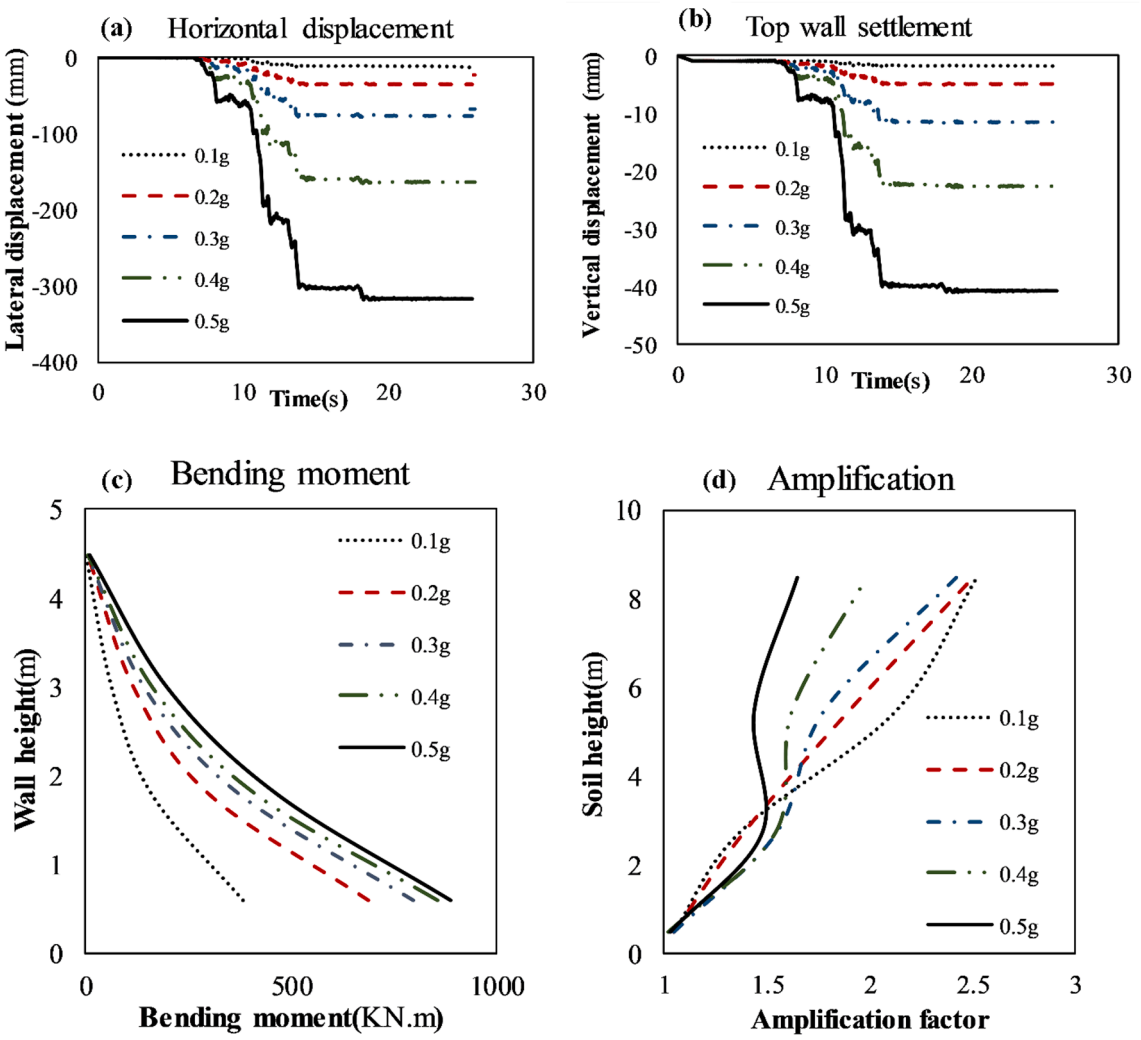

Fig. 12. Effect of acceleration value on: (a) Lateral displacement of top wall; (b) Vertical displacement of top wall; (c) Bending moment; (d) Amplification pattern.

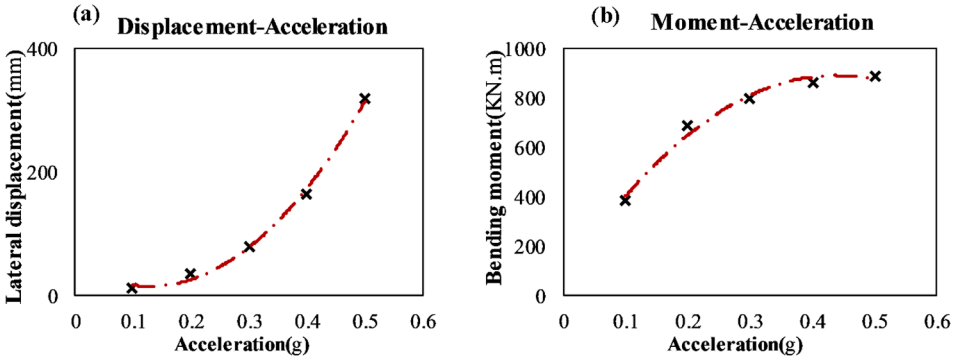

Fig. 13. Trend of parameters to acceleration: (a) Residual lateral displacement; (b) Bending moment.

recorded. The effects of input motion PGA, backfill and foundation mechanical properties and frequency content of ground motion were examined and reported.

The following conclusions are drawn based on the physical properties of the materials and soil model used in the present study:

(1) Ground motions with the forward directivity pulse, induced very large residual displacements into the cantilever retaining walls. The main part of displacement occurred in a narrow bandwidth of time, due to the pulse effect. Eliminating this pulse through the wavelet method considerably reduced the maximum lateral displacements.
(2) The results showed that the near-fault ground motions and far-field records imposed approximately identical moment values to the wall. This fact illustrates that distribution of force behind the wall is not only design parameter.
(3) The retaining wall under near-source earthquakes with PGAs 0.1 g to 0.3 g, experienced horizontal displacements lower than the

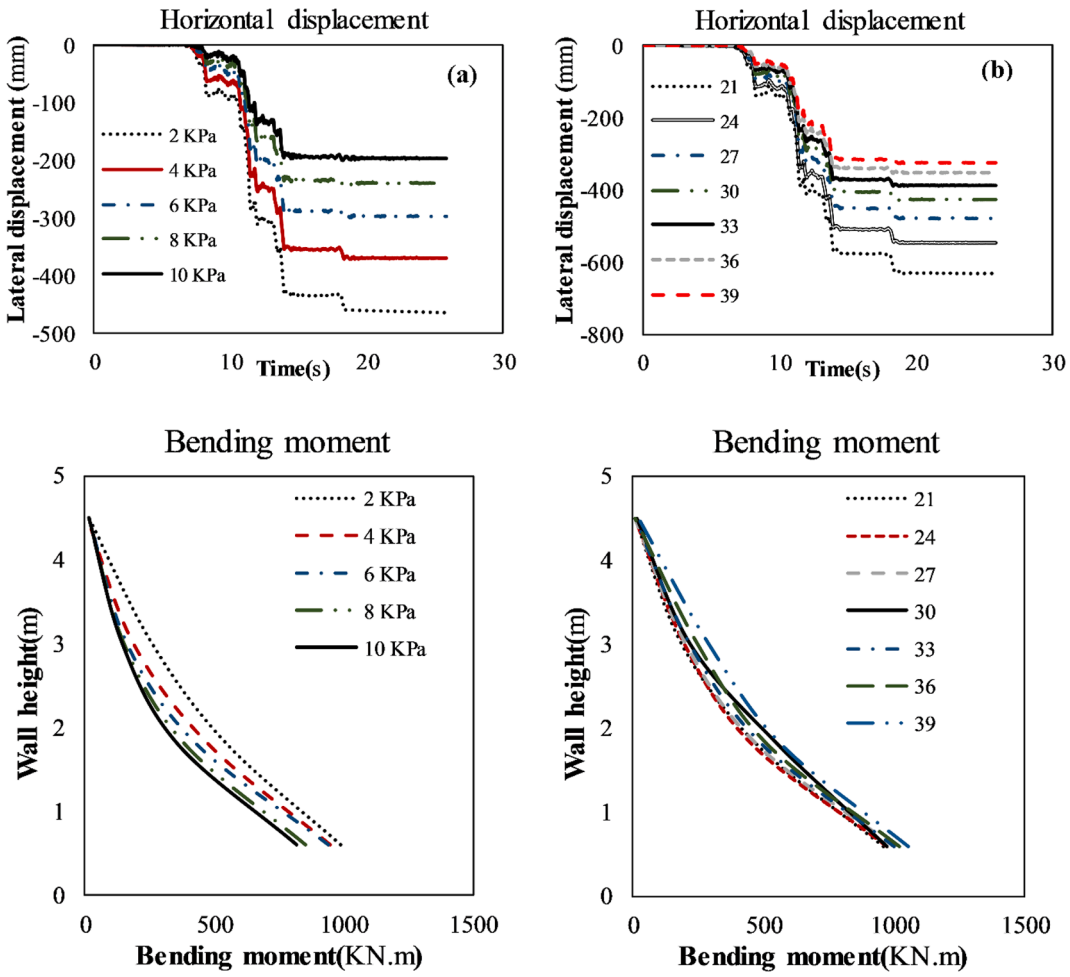

Fig. 14. Seismic response of retaining wall based on backfill properties (a) Cohesion; (b) friction angle.

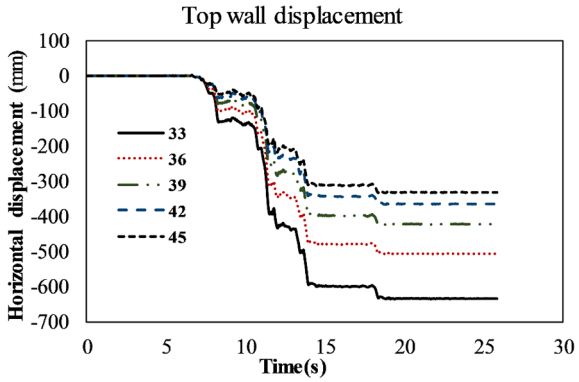

Fig. 15. Seismic response of retaining wall based on foundation friction angle.

permissible and failure states based on criteria reported in table4 in particular, Huang et al. (2009). The lateral displacements under records with PGA = 0.4 g were almost larger than the permissible state. The residual displacements exceeded from 5% of the wall height for earthquakes with PGAs more than 0.5 g and the failure condition happened.

(4) Lower displacements were recorded for generated far-field records, although the failure state was observed for records with PGA = 0.6 g.

(5) The rotation of wall had a reverse correlation with free field PGA. Models under smaller PGAs had a larger magnitude of rotation. Sliding was, therefore, considered as the main failure mechanism in strong ground motions.

(6) The ratio of PGV/PGA had an undeniable effect on the response of the system. The results showed that, with same strong ground motion properties including PGA, duration and faulting mechanisms, system response depends strongly on PGV/PGA values. A higher value of displacement was observed in records with larger PGV/PGA magnitudes, even in cases where the bending moment distribution was lowest.

(7) A comparison between the results and the literature shows that if soil properties remain constant, wall movement will be affected by both the PGA and the velocity of records and not only PGA value.

Table 7
Main properties of "Imperial Valley-06" selected stations.

Station	RSN number	PGV (cm/s)	Rrup (km)	Arias intensity (m/s)	Tp (s)	PGV/PGA (s)
"El Centro - Meloland Geot. Array"	171	92.7	0.07	1.105	0.56	0.302
"El Centro Differential Array"	184	26.67	5.09	0.831	0.4	0.087
"El Centro Array #12"	175	44.5	17.94	1.709	0.2	0.151

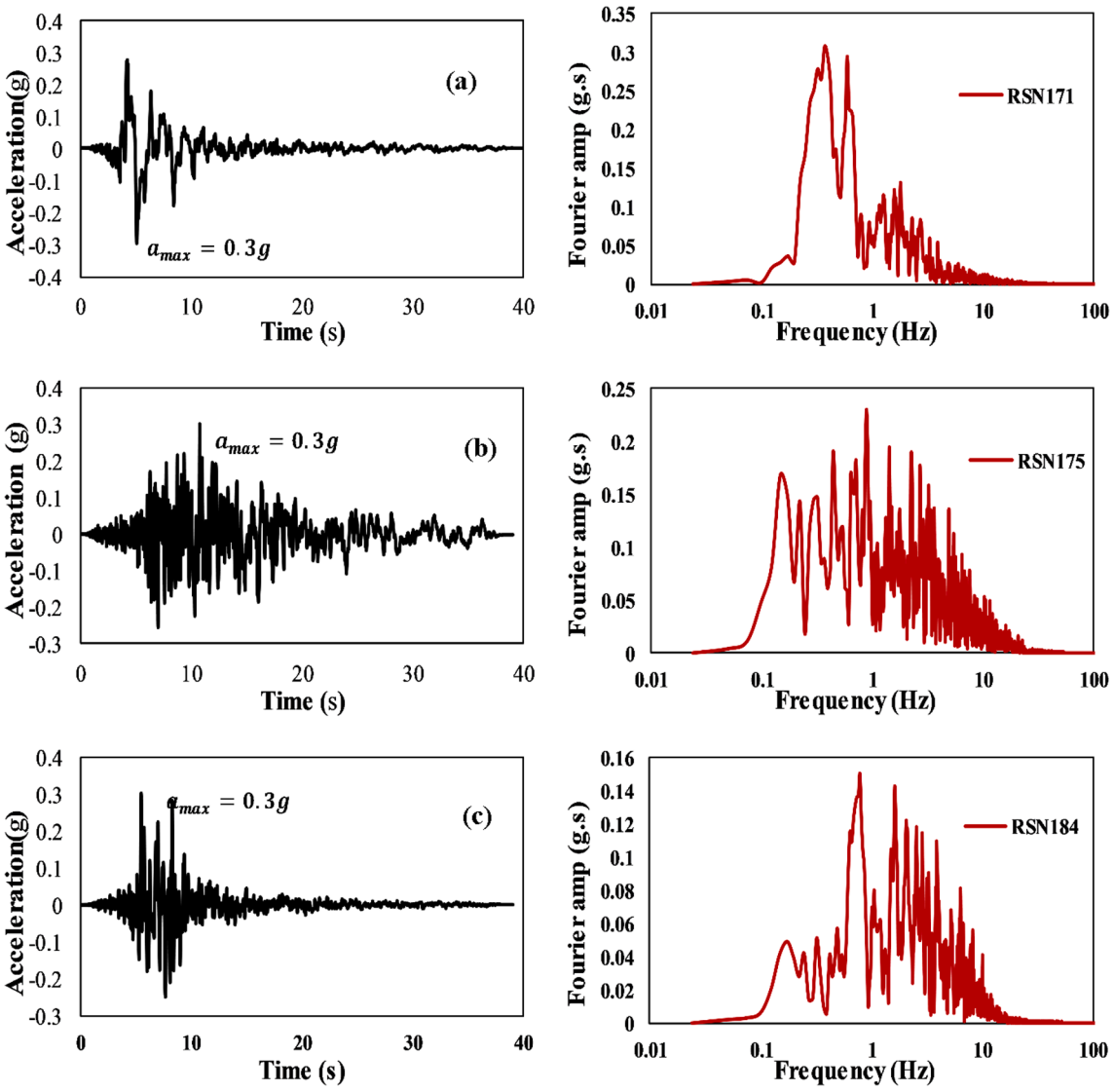

Fig. 16. Imperial Valley-06 scaled acceleration time histories and Fourier spectrum recorded during shaking at station: (a) "El Centro - Meloland Geot. Array"; (b) "El Centro Array #12"; (c) "El Centro Differential Array"

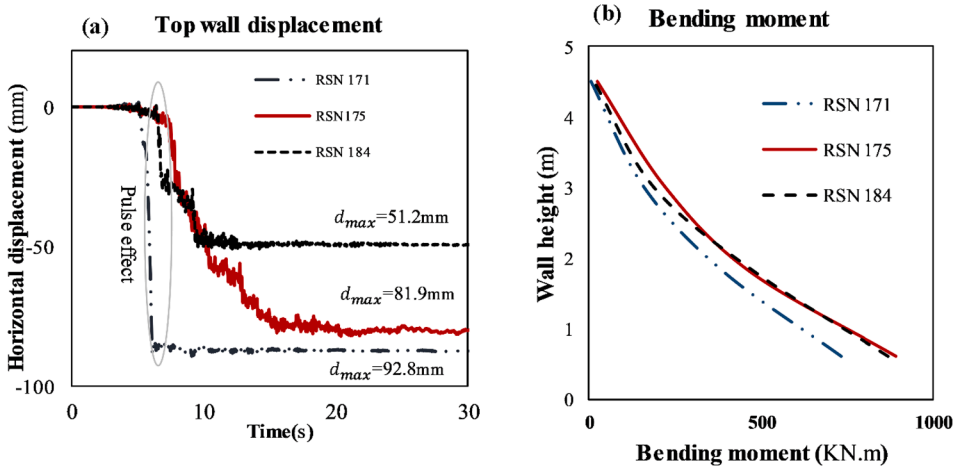

Fig. 17. Effect of frequency content on Seismic response of retaining wall (a) Lateral displacement; (b) Bending moment.

CRediT authorship contribution statement

Milad Aghamolaei: Software, Validation, Formal analysis, Writing - original draft. **Alireza Saeedi Azizkandi:** Conceptualization, Methodology, Supervision. **Mohammad Hassan Baziar:** Conceptualization, Methodology, Supervision. **Sadegh Ghavami:** Writing - review & editing.

Declaration of Competing Interest

The authors declare that they have no known competing financial interests or personal relationships that could have appeared to influence the work reported in this paper.

Appendix A. Supplementary material

Supplementary data to this article can be found online at https://doi.org/10.1016/j.compgeo.2020.103924.

References

Alavi, Babak, Krawinkler, Helmut, 2000. Consideration of near-fault ground motion effects in seismic design. In: Proceedings of the 12th World Conference on Earthquake Engineering, 8, 2000.

American Association of State Highway and Transportation Officials AASHTO, 2002. Standard specifications for highway bridges, Secs. 3 and 7, Washington, D.C.

Anastasopoulos, I., Gazetas, G., Bransby, M.F., Davies, M.C.R., El Nahas, A., 2007. Fault rupture propagation through sand: Finite-element analysis and validation through centrifuge experiments. J. Geotech. Geoenviron. Eng. 133 (8), 943–958.

Al Atik, Linda, Sitar, Nicholas, 2010. Seismic earth pressures on cantilever retaining structures. J. Geotech. Geoenviron. Eng. 136(10), 1324–1333.

Baker, Jack W., 2007. Quantitative classification of near-fault ground motions using wavelet analysis. Bull. Seismol. Soc. Am. 97 (5), 1486–1501.

Bakr, Junied, Ahmad, Syed Mohd, 2018. A Finite element performance-based approach to correlate movement of a rigid retaining wall with seismic earth pressure. Soil Dyn. Earthquake Eng. 114, 460–479.

Bakr, Junied, Ahmad, Syed Mohd, Lombardi, Domenico, 2019. Finite-element study for seismic structural and global stability of cantilever-type retaining walls. Int. J. Geomech. 19 (10), 04019117.

Baziar, M.H., Rostami, H., 2017. Earthquake demand energy attenuation model for liquefaction potential assessment. Earthq. Spectra 33 (2), 757–780.

Bertero, V.V., Mahin, S.A., Herrera, R.A., 1978. Aseismic design implications of near-fault San Fernando earthquake records. Earthq. Eng. Struct. Dyn. 6 (1), 31–42.

Brandenberg, Scott J., Mylonakis, George, Stewart, Jonathan P., 2017. Approximate solution for seismic earth pressures on rigid walls retaining inhomogeneous elastic soil. Soil Dyn. Earthquake Eng. 97, 468–477.

Bray, Jonathan D., Rodriguez-Marek, Adrian, 2004. Characterization of forward-directivity ground motions in the near-fault region. Soil Dyn. Earthq. Eng. 24(11), 815–828.

Cakir, Tufan, 2013. Evaluation of the effect of earthquake frequency content on seismic behavior of cantilever retaining wall including soil-structure interaction. Soil Dyn. Earthquake Eng. 45, 96–111.

Cakir, Tufan, 2014. Backfill and subsoil interaction effects on seismic behavior of a cantilever wall. Geomech. Eng. 6 (2), 117–138.

Candia, Gabriel, Mikola, Roozbeh Geraili, Sitar, Nicholas, 2016. Seismic response of retaining walls with cohesive backfill: centrifuge model studies. Soil Dyn. Earthquake Eng. 90, 411–419.

Conti, R., Caputo, G., 2019. A numerical and theoretical study on the seismic behaviour of yielding cantilever walls. Géotechnique 69 (5), 377–390.

Conti, R., Madabhushi, G.S.P., Viggiani, G.M.B., 2012. On the behaviour of flexible retaining walls under seismic actions. Géotechnique 62 (12), 1081.

Davoodi, M., Jafari, M.K., Hadiani, N., 2013. Seismic response of embankment dams under near-fault and far-field ground motion excitation. Eng. Geol. 158, 66–76.

Deyanova, Manya, Lai, Carlo G., Martinelli, Mario, 2016. Displacement–based parametric study on the seismic response of gravity earth-retaining walls. Soil Dyn. Earthquake Eng. 80, 210–224.

di Santolo, Anna Scotto, Evangelista, Aldo, 2011. Dynamic active earth pressure on cantilever retaining walls. Comput. Geotech. 38(8) 1041–1051.

Garini, E., Tsantilas, L., Gazetas, G., 2016. Seismic response of cantilever retaining walls: verification of centrifuge experiments. Proceedings of the 1st ICONHIC (207).

Garini, E., Gazetas, G., 2013. Damage Potential of near-Fault Records: Sliding Displacement against Conventional "Intensity Measures". Bull. Earthq. Eng. 11 (2), 455–480.

Gazetas, George, Garini, Evangelia, Anastasopoulos, I., Georgarakos, T., 2009. Effects of near-fault ground shaking on sliding systems. J. Geotech. Geoenviron. Eng. 135(12), 1906–1921.

Gazetas, G., Psarropoulos, P.N., Anastasopoulos, I., Gerolymos, N., 2004. Seismic behaviour of flexible retaining systems subjected to short-duration moderately strong excitation. Soil Dyn. Earthquake Eng. 24 (7), 537–550.

Green, Russell A., Guney Olgun, C., Cameron, Wanda I., 2008. Response and modeling of cantilever retaining walls subjected to seismic motions. Comput.-Aided Civ. Infrastruct. Eng. 23 (4), 309–322.

Hall, J.F., Heaton, T.H., Halling, M.W., Wald, D.J., 1995. Near-source ground motion and its effects on flexible buildings. Earthq. Spectra 11 (4), 569–605.

Hayden, Connor P., Bray, Jonathan D., Abrahamson, Norman A., 2014. Selection of near-Fault Pulse Motions. J. Geotech. Geoenviron. Eng. 140 (7), 04014030.

Huang, C.-C., Wu, S.-H., Wu, H.-J., 2009. Seismic displacement criterion for soil retaining walls based on soil strength mobilization. J. Geotech. Geoenviron. Eng. 135 (1), 74–83.

Iai, S., Tobita, T., Nakahara, T., 2005. Generalised scaling relations for dynamic centrifuge tests. Geotechnique 55 (5), 355–362.

Jadhav, Prajakta R., Prashant, Amit, 2020. Computation of seismic translational and rotational displacements of cantilever retaining wall with shear key. Soil Dyn. Earthquake Eng. 130, 105966.

Jo, Seong-Bae, Ha, Jeong-Gon, Lee, Jin-Sun, Kim, Dong-Soo, 2017. Evaluation of the seismic earth pressure for inverted T-shape stiff retaining wall in cohesionless soils via dynamic centrifuge. Soil Dyn. Earthquake Eng. 92, 345–357.

Ju, Shen-Haw, Ni, Sheng-Huoo, 2007. Determining Rayleigh damping parameters of soils for finite element analysis. Int. J. Numer. Anal. Meth. Geomech. 31 (10), 1239–1255.

Kalkan, Erol, Kunnath, Sashi K., 2006. Effects of fling step and forward directivity on seismic response of buildings. Earthq. Spectra 22 (2), 367–390.

Kloukinas, Panos, Penna, Augusto, di Santolo, Anna Scotto, Bhattacharya, Subhamoy, Dietz, Matt S., Dihoru, Luiza, Evangelista, Aldo, Simonelli, Armando L., Taylor, Colin A., Mylonakis, George, 2014. Experimental investigation of dynamic behavior of cantilever retaining walls. In: Seismic Evaluation and Rehabilitation of Structures, 477-493: Springer, 2014.

Kloukinas, Panos, di Santolo, Anna Scotto, Penna, Augusto, Dietz, Matthew, Evangelista, Aldo, Simonelli, Armando Lucio, Taylor, Colin, Mylonakis, George, 2015. Investigation of seismic response of cantilever retaining walls: limit analysis vs shaking table testing. Soil Dyn. Earthq. Eng. 77 (2015) 432–445.

Kuhlemeyer, Roger L., Lysmer, John, 1973. Finite element method accuracy for wave propagation problems. J. Soil Mech. Foundations Div 99, no. Tech Rpt (1973).

Lysmer, John, Kuhlemeyer, Roger L, 1969. Finite dynamic model for infinite media. J. Eng. Mech. Division 95 (4), 859–878.

Madabhushi, S.P.G., Zeng, X., 2007. Simulating seismic response of cantilever retaining walls. J. Geotech. Geoenviron. Eng. 133 (5), 539–549.

Mavroeidis, George P., Papageorgiou, Apostolos S., 2003. A mathematical representation of near-fault ground motions. Bull. Seismol. Soc. Am. 93 (3), 1099–1131.

Mikola, Geraili, Roozbeh, Gabriel Candia, Sitar, Nicholas, 2016. Seismic earth pressures on retaining structures and basement walls in cohesionless soils. J. Geotech. Geoenviron. Eng. 142 (10), 04016047.

Mollaioli, Fabrizio, Bosi, Anna, 2012. Wavelet analysis for the characterization of forward-directivity pulse-like ground motions on energy basis. Meccanica 47 (1), 203–219.

Mononobe, N., Matsuo, H., 1929. On the determination of earth pressures during earthquakes. Volume 9, Tokyo, 1929." In World Engineering Congress.

Mukhopadhyay, S., Gupta, V.K., 2013. Directivity pulses in near-fault ground motions—I: Identification, extraction and modeling. Soil Dyn. Earthq. Eng. 50, 1–15.

Nakamura, Shinya, 2006. Reexamination of mononobe-okabe theory of gravity retaining walls using centrifuge model tests. Soils Found. 46 (2), 135–146.

Nimbalkar, Sanjay, Choudhury, Deepankar, 2007. Sliding stability and seismic design of retaining wall by pseudo-dynamic method for passive case. Soil Dyn. Earthquake Eng. 27 (6), 497–505.

Okabe, Saburo, 1924. General Theory on Earth Pressure and Seismic Stability of Retaining Wall and Dam. Proc. Civil Engrg. Soc., Japan 10 (6), 1277–1323.

Osouli, Abdolreza, Zamiran, Siavash, 2017. The effect of backfill cohesion on seismic response of cantilever retaining walls using fully dynamic analysis. Comput. Geotech. 89, 143–152.

Psarropoulos, P.N., Klonaris, G., Gazetas, G., 2005. Seismic earth pressures on rigid and flexible retaining walls. Soil Dyn. Earthquake Eng. 25 (7–10), 795–809.

Salem, Abdelwahhab N., Ezzeldine, Omar Y., Amer, Mohamed I., 2020. Seismic loading on cantilever retaining walls: Full-scale dynamic analysis. Soil Dyn. Earthquake Eng. 130, 105962.

Santhoshkumar, G., Ghosh, Priyanka, Murakami, Akira, 2019. Seismic active resistance of a tilted cantilever retaining wall considering adaptive failure mechanism. Int. J. Geomech. 19 (8), 04019086.

Seed, H., 1970. Design of earth retaining structures for dynamic loads. In: ASCE Specialty Conf.-Lateral Stress in the Ground and Design of Earth Retaining Structures, 1970, 1970.

Somerville, P.G., 2003. Magnitude scaling of the near fault rupture directivity pulse. Phys. Earth Planet. Inter. 137 (1–4), 201–212.

Somerville, P.G., Smith, N.F., Graves, R.W., Abrahamson, N.A., 1997. Modification of empirical strong ground motion attenuation relations to include the amplitude and duration effects of rupture directivity. Seismol. Res. Lett. 68 (1), 199–222.

Song, Jian, Rodriguez-Marek, Adrian, 2014. Sliding Displacement of Flexible Earth Slopes Subject to near-Fault Ground Motions. J. Geotech. Geoenviron. Eng. 141 (3), 04014110.

The Commission of the European Communities European prestandard, 1994. Eurocode 8: Design provisions for earthquake resistance of structures—Part 5: Foundations, retaining structures and geotechnical aspects. Brussels.

Vassiliou, Michalis F, Makris, Nicos, 2011. Estimating time scales and length scales in pulselike earthquake acceleration records with wavelet analysis. Bull. Seismol. Soc. Am. 101 (2), 596–618.

Veletsos, Anestis S., Younan, Adel H., 1997. Dynamic response of cantilever retaining walls. J. Geotech. Geoenviron. Eng. 123 (2), 161–172.

Wu, Yingwei, Prakash, Shamsher, 1996. On seismic displacements of rigid retaining walls. In: Analysis and Design of Retaining Structures against Earthquakes, 21–37.
Zamiran, Siavash, Osouli, Abdolreza, 2018. Seismic motion response and fragility analyses of cantilever retaining walls with cohesive backfill. Soils Found. 58 (2), 412–426.
Zou, Degao, Han, Huichao, Liu, Jingmao, Yang, Dixiong, Kong, Xianjing, 2017. Seismic Failure Analysis for a High Concrete Face Rockfill Dam Subjected to near-Fault Pulse-Like Ground Motions. Soil Dyn. Earthquake Eng. 98, 235–243.